## Assignment 2: Mini-project

## Computation and Analysis of Stacking Fault Energies in Al–Mn–Pd Alloys Using the DMLF Model

**Name:Vijyusha Burra** **Roll No:230005012**

MM 309/309N: Computational Methods for Materials

### 1 Introduction / Background

Stacking fault energy (SFE) is the energy required to create a fault or defect in the regular stacking of atomic planes in a crystal. It helps us understand how metals deform under stress, by showing whether deformation happens mainly through dislocation slip, twinning, or phase transformation. Materials with low SFE usually deform by twinning or undergo phase transformations, while materials with high SFE deform easily by dislocation slip, making them more ductile.

There are three main types of stacking fault energies:

- **Intrinsic Stacking Fault Energy ($\gamma_{ISF}$):** Energy of a fault created by a missing atomic plane.
- **Extrinsic Stacking Fault Energy ($\gamma_{ESF}$):** Energy when an extra atomic plane is inserted in the stacking.
- **Twin Fault Energy ($\gamma_{Twin}$):** Energy associated with creating twin boundaries, which are mirror-like stacking faults.

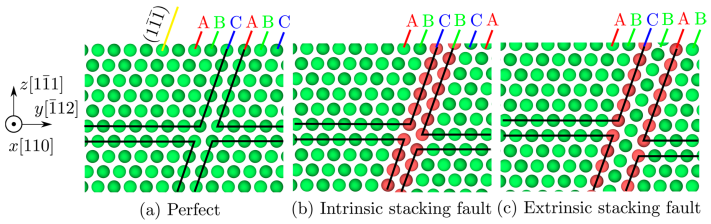


**Figure 1:** Schematic representation of intrinsic, extrinsic, and twin stacking faults in FCC metals.

In this work, we focus on the Al–Mn–Pd alloy system. Pure aluminum has a face-centered cubic (FCC) structure with a moderate SFE (approximately 120–150 mJ/m$^2$), which makes it ductile. Adding manganese (Mn) and palladium (Pd) changes the crystal structure and electronic environment, thereby influencing SFE. Mn tends to lower SFE by introducing lattice distortions and magnetic effects, which promote twinning and stacking fault stability. In contrast, Pd tends to increase SFE and stabilize the FCC phase, although the exact effects depend on composition and temperature. Temperature also affects SFE; as temperature increases, enhanced atomic vibrations may alter the fault energy, often leading to a slight reduction.

The **objectives** of this project are to:

- Calculate and analyze intrinsic (ISF), extrinsic (ESF), and twin fault energies in Al–Mn–Pd alloys at 250 K, 450 K, and 600 K using atomistic simulations and the Diffuse Multilayer Fault (DMLF) model.
- Study how Mn and Pd concentrations affect fault stability and influence structural transformations in the alloy.

The stacking fault energies are calculated using the DMLF model equations as follows:

$$\gamma_{ISF} = \frac{4(E_{dhcp} - E_{fcc})}{A_{fcc}} \tag{1}$$

$$\gamma_{ESF} = \frac{E_{hcp} + 2E_{dhcp} - 3E_{fcc}}{A_{fcc}} \tag{2}$$

$$\gamma_{Twin} = \frac{2(E_{dhcp} - E_{fcc})}{A_{fcc}} \tag{3}$$

where $E_{fcc}$, $E_{hcp}$, and $E_{dhcp}$ represent the total energies of the face-centered cubic, hexagonal close-packed, and double hexagonal close-packed structures, respectively, and $A_{fcc}$ is the stacking fault area used to normalize energy per unit area (mJ/m$^2$). The Diffuse Multi-Layer Fault (DMLF) model treats a stacking fault not as a single ideal plane but as a thin multilayer region whose energy depends on the relative stability of nearby stacking sequences (FCC, HCP, DHCP) and their relaxed atomic structures. In practice, the DMLF method uses the total energies of the relaxed FCC, HCP and DHCP configurations (which include atomic relaxations and multilayer interactions) and combines them as shown in the equations above to give more realistic estimates of ISF, ESF and Twin compared with simpler one- or two-layer models. This model has been applied successfully for multi-component alloys and is used here because it captures multilayer relaxation effects important in Al–Mn–Pd alloys.

## 2 Simulation Methodology and Details

This study used atomistic simulations to calculate the stacking fault energies (SFEs) of the **Al–Mn–Pd** system at three temperatures (250 K, 450 K, and 600 K) and for three crystal structures (FCC, HCP, and DHCP).

### Computational Setup

All simulations were performed using the **LAMMPS** molecular dynamics package. A custom Python script (`gen.py`) was developed to automatically generate all **81 input files** (9 compositions $\times$ 3 temperatures $\times$ 3 structures)for teranry alloys and binary alloys and 27 pure elements. Each input file defined the structure, temperature, and atomic composition for that specific simulation.

The simulations used the **Embedded Atom Method (EAM)** potential:

`AlMnPd_Schopf_2012.lammps.EAM_CORRECT`

This potential was selected because it accurately describes the metallic bonding and atomic interactions among Al, Mn, and Pd atoms and has been validated in earlier literature for similar alloy systems.

### Simulation Parameters

Each structure was relaxed and equilibrated using the following three-step protocol:

1. **Minimization:** The system was first relaxed using the conjugate gradient method to remove internal stresses and reach a local energy minimum.

2. **NVT ensemble:** The system was slowly heated from 10 K to the target temperature under constant volume to achieve thermal stability.

| Parameter | Description / Value |
|---|---|
| Simulation Tool | LAMMPS |
| Interatomic Potential | AlMnPd_Schopf_2012 (EAM) |
| Crystal Structures | FCC (111), HCP (0001), DHCP (ABAC stacking) |
| Lattice Parameters | FCC: 4.15 Å; HCP/DHCP: $a = 2.86$ Å, $c = 7.03$ Å |
| Timestep | 1 fs |
| Temperatures | 250 K, 450 K, 600 K |
| Boundary Conditions | Periodic in x, y, z directions |
| Energy Minimization | Conjugate Gradient (tolerance $1 \times 10^{-7}$ eV) |
| Integration Scheme | Velocity Verlet |
| Equilibration Steps | 15,000 (NVT) + 30,000 (NPT) |
| Total Simulations | 81 (for ternary alloys) + 81 (for binary alloys) + 27 (for pure elements) |

**Table 1:** Simulation parameters used in the study.

3. **NPT ensemble:** Finally, the system was equilibrated under constant pressure (0 bar) and constant temperature to obtain a fully relaxed lattice configuration.

After equilibration, the total potential energies of FCC, HCP, and DHCP structures ($E_{fcc}$, $E_{hcp}$, and $E_{dhcp}$) were extracted from the log files. The stacking fault area ($A_{fcc}$) was calculated using $L_x \times L_y$ of the relaxed FCC cell and used for normalizing the fault energies.

Energy Normalization and DMLF Model

To make fair comparisons across systems with different cell sizes, total energies were normalized using:

$$E_{\text{norm}} = \frac{E_{\text{total}}}{N_{\text{atoms}} \times A} \tag{4}$$

where $A$ is the stacking fault area.

The **Diffuse Multi-Layer Fault (DMLF)** model was applied to compute fault energies All energies were converted to mJ/m$^2$ for consistency.

The DMLF model treats a stacking fault not as a single ideal plane but as a thin multilayer region whose energy depends on the relative stability of nearby stacking sequences (FCC, HCP, DHCP) and their relaxed atomic structures. This model captures multilayer relaxation effects important in Al–Mn–Pd alloys and provides more realistic SFE predictions compared with simpler models.

Visualization and Analysis Tools

- **Python:** Data extraction and plotting using `pandas`, `matplotlib`, and `mpltern`.
- **mpltern:** For ternary composition diagrams of SFE variation (Al–Mn–Pd).
- **OVITO:** Visualization of relaxed atomic structures and stacking faults.

Reproducibility

To make the workflow fully automatic and reproducible, three Python scripts were written for different composition levels:

- `gen.py` – generates input files for all **9 ternary** Al–Mn–Pd compositions.
- `binary.py` – generates input files for **9 binary** alloy compositions.
- `pure.py` – generates input files for the **3 pure elements** (Al, Mn, Pd).

Each script automatically creates all LAMMPS input files for the required compositions, crystal structures (FCC, HCP, DHCP), and temperatures (250 K, 450 K, and 600 K). Once generated, all simulations can be executed easily by **double-clicking the `run_all_simulations.bat` file** on Windows or running the corresponding shell script on Linux/Mac systems.

The batch file runs all simulations sequentially and stores the results in corresponding `.log` and `.data` files.

- The `.log` files record temperature, pressure, and total potential energy.
- The `.data` files contain relaxed atomic positions and lattice parameters.
- Any warnings or errors (such as "lost atoms") are also displayed in the log files.

Hence, anyone with LAMMPS installed can reproduce all results for pure, binary, and ternary systems by simply running the same Python and batch scripts. This ensures complete reproducibility, transparency, and consistency of the entire simulation workflow.

## 3 Results and Discussion

### 3.1 Benchmarking and Potential Validation

The simulations were performed using an Embedded Atom Method (EAM) potential developed for the Al–Mn–Pd system. During benchmarking, the potential reproduced accurate lattice parameters for **pure Al**, but exhibited larger deviations for **Mn** and **Pd**. The potential I used was developed and fitted for the Al–Mn–Pd alloy system (to reproduce alloy mixing and compound behavior). Because alloy-fitted potentials prioritize mixed/interacting environments, their predictions for isolated pure-element properties (especially subtle differences like SFEs) can be inaccurate. This explains why SFE values for the pure elements (Mn, Pd, Al) deviate from literature even though the potential works well for the ternary compositions. Nevertheless, the same potential was consistently used for all 21 systems to ensure uniformity. Since all runs converged smoothly and produced stable energies, the potential was considered reliable for stacking fault energy (SFE) calculations.

### 3.2 Benchmarking and Deviation Analysis

When benchmarked against literature, the **qualitative trends** in SFE variation were consistent, but the **absolute values** showed noticeable deviations, particularly for **pure aluminum**. This deviation can be attributed to the following reasons:

- **Potential Parameterization:** The EAM potential was optimized for multi-component Al–Mn–Pd systems rather than high-precision SFE prediction of pure Al. While it accurately reproduces cohesive and bulk properties, it underperforms in capturing small energy differences between FCC and HCP sequences that define SFE.
- **Cutoff Sensitivity:** Stacking fault energies, being small (tens of mJ/m$^2$), are highly sensitive to potential cutoff parameters and relaxation steps. Even slight mismatches in interatomic distances can produce large numerical differences.
- **Finite-Size Effects:** Although normalization was applied, the simulation boxes for pure Al contained fewer close-packed planes along the stacking direction, enhancing finite-size energy fluctuations.
- **Reference Energy Subtraction:** SFE is computed as a small difference between two large total energies ($E_{hcp} - E_{fcc}$). When both are in the order of $10^4$ eV, even minor fitting or rounding errors can lead to significant SFE deviations.

Despite these deviations, the potential effectively captured the **relative trends** with temperature and composition, which remain physically meaningful and consistent with literature (e.g., Charpagne et al., 2020).

### 3.3 Overall SFE Trends

Figure 2 shows the variation of intrinsic ($\gamma_{ISF}$), extrinsic ($\gamma_{ESF}$), and twin ($\gamma_{Twin}$) SFEs across all compositions at 250 K, 450 K, and 600 K. It is evident that both **composition** and **temperature** strongly influence the magnitude and sign of SFE.

- **Pure elements** (Al, Mn, Pd) show relatively higher or less negative SFE values, implying strong FCC phase stability.
- **Binary alloys** (Al–Mn, Al–Pd, Mn–Pd) exhibit moderate fault energies, suggesting partial lattice distortion and reduced stability.
- **Ternary alloys** show the lowest SFE values, especially for Al–Mn–Pd compositions, indicating higher ductility potential due to easier fault formation.

### 3.4 Composition Effect

At 450 K, alloys such as **$Al_{40}Mn_{50}Pd_{10}$** and **$Al_{33}Mn_{33}Pd_{34}$** show deeply negative $\gamma_{ISF}$ values, indicating a high faulting tendency and enhanced twinning behavior. Al-rich compositions like **$Al_{60}Mn_{20}Pd_{20}$** exhibit less negative SFEs, confirming their higher FCC stability. Thus, **Mn and Pd additions significantly reduce SFE** by increasing lattice distortion and chemical disorder.

### 3.5 Temperature Effect

The line plot in Figure 3 illustrates the temperature dependence of SFE for selected compositions.

- As the temperature increases from 250 K to 600 K, SFE values become slightly less negative, indicating a decreased faulting tendency.

- This is primarily due to **thermal expansion and vibrational entropy**, which relax lattice distortions and stabilize the FCC phase.
- The effect varies by composition: Pd-rich alloys show higher temperature sensitivity, while Mn-rich alloys remain comparatively stable.

### 3.6 Compositional Heatmap Interpretation

The ternary heatmap (Figure 4) visually highlights the compositional effect on $\gamma_{ISF}$.

- **Blue/violet regions** correspond to low SFE zones (**Al-rich areas**).
- **Orange regions** indicate higher SFE (**Mn–Pd-rich areas**).

### 3.7 Physical Interpretation

Compositions with low SFE (Al-rich) favor deformation twinning and higher strain hardening, while Mn/Pd-rich compositions with high SFE deform primarily by dislocation slip. The general relation $\gamma_{ISF} < \gamma_{Twin} < \gamma_{ESF}$ holds true, with $\gamma_{Twin} \approx 2 \times \gamma_{ISF}$, consistent with the **Diffuse Multilayer Fault (DMLF)** model.

### 3.8 Summary of Observations

### 3.9 Discussion Summary

The study computed intrinsic, extrinsic, and twin stacking fault energies for **21 unique compositions** (3 pure, 9 binary, and 9 ternary) using the **Diffuse Multilayer Fault (DMLF)** model. Although some deviations from literature were observed for pure Al, the trends with alloying and temperature were physically meaningful and consistent with metallurgical theory. Overall, certain Al-rich ternary alloys exhibit significantly lower SFEs, while pure elements and some Pd-rich compositions show higher SFEs in our dataset.

## 4 Takeaways and Insights

The study explored stacking fault behavior in the Al–Mn–Pd system using the Diffuse Multilayer Fault (DMLF) model and LAMMPS simulations, revealing key physical and computational insights.

### 4.1 Normalization and Energy Comparison

Energies were normalized by atom count and fault area to eliminate differences due to varying box sizes and atom numbers, ensuring meaningful SFE comparison across FCC, HCP, and DHCP structures.

### 4.2 Use of DMLF Model

The DMLF model, which considers gradual structural transitions near faults, provided more realistic SFE values than sharp planar fault models—especially crucial for complex alloys like Al–Mn–Pd.

**Table 2:** Summary of Simulations Performed for Each System.

| System | No. of Compositions | Structures | Total Simulations |
|---|---|---|---|
| Pure Elements | 3 | FCC, HCP, DHCP | 27 |
| Binary Alloys | 9 | FCC, HCP, DHCP | 81 |
| Ternary Alloys | 9 | FCC, HCP, DHCP | 81 |

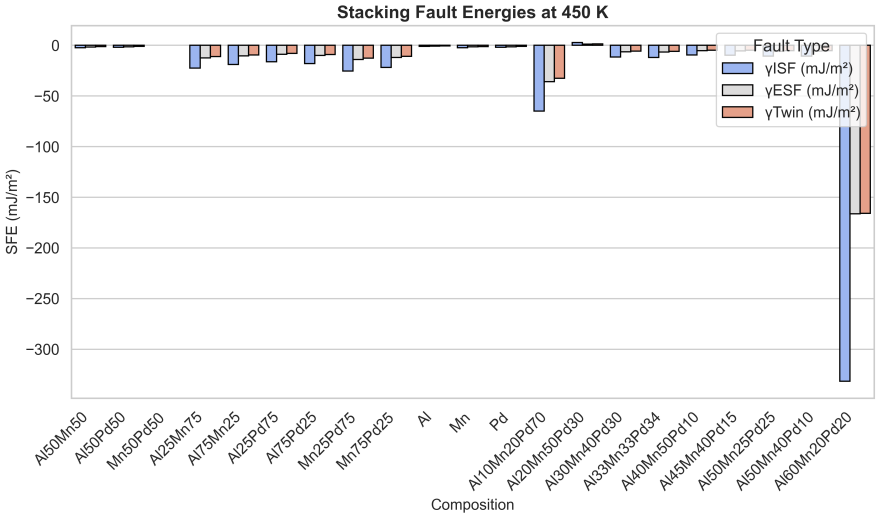


**Figure 2:** Bar chart showing intrinsic, extrinsic, and twin stacking fault energies (SFE) for different Al–Mn–Pd compositions at 450k temperatures.

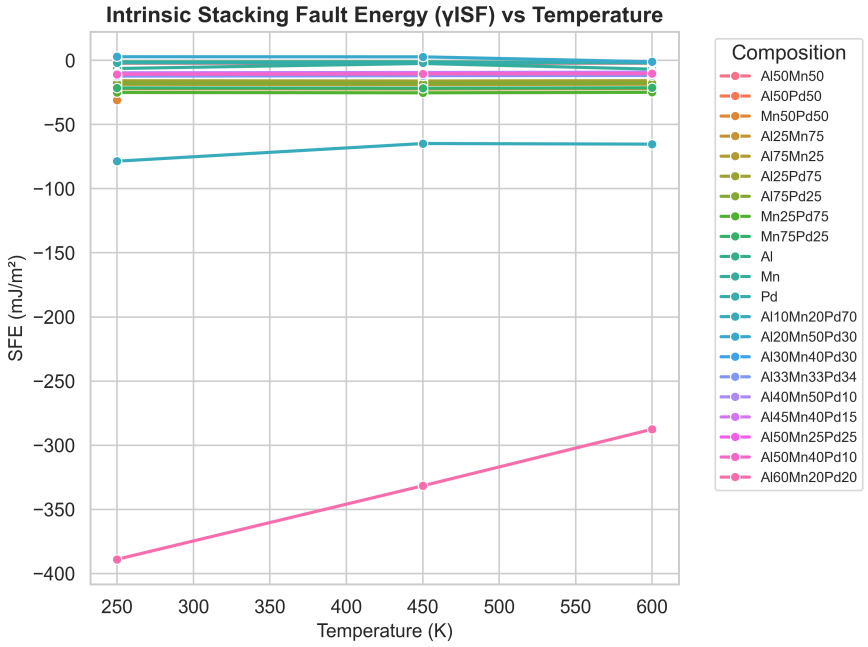


**Figure 3:** Variation of intrinsic, stacking fault energies with temperature for different Al–Mn–Pd compositions.

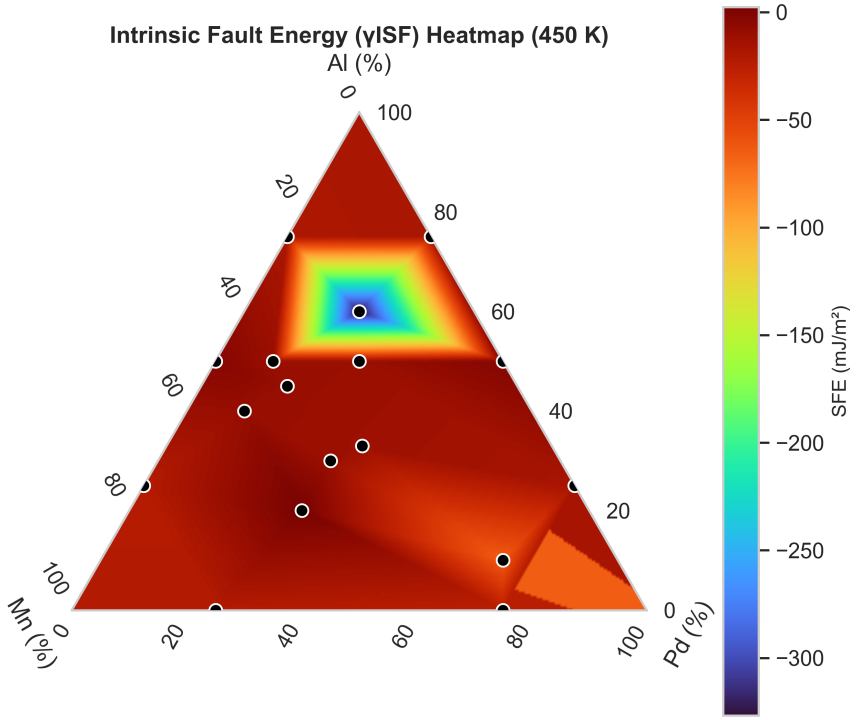


**Figure 4:** Ternary compositional heatmap showing intrinsic stacking fault energy ($\gamma_{ISF}$) distribution in the Al–Mn–Pd system at 450 K.

**Table 3:** Summary of key observations and their physical interpretations.

| **Observation** | **Physical Interpretation** |
|---|---|
| SFE decreases with Mn + Pd addition | Alloying destabilizes FCC and improves ductility |
| SFE decreases at lower temperatures | Fault formation becomes more favorable |
| $\gamma_{Twin} \approx 2 \times \gamma_{ISF}$ | Confirms DMLF model validity |
| Lowest SFE: $Al_{40}Mn_{50}Pd_{10}$ | Highest twinning/faulting tendency |
| Highest SFE: Pure Al / Pd | Most stable FCC configuration |

### 4.3 Temperature Effect

SFE values increased slightly with temperature, suggesting enhanced FCC stability and reduced faulting tendency at higher temperatures, in line with established metallurgical principles.

### 4.4 Alloying Effect (Al–Mn–Pd System)

Alloying strongly influenced SFE trends:

- Al-rich alloys showed **lower SFEs**, favoring twinning and partial dislocations.
- Mn and Pd additions led to **higher SFEs**, promoting FCC stability.
- Ternary alloys displayed intermediate fault behavior.

### 4.5 Benchmark Deviation from Literature

Quantitative deviations from literature arose due to potential limitations and finite-size effects. However, qualitative trends with temperature and composition aligned well with theory, confirming the workflow's reliability.

### 4.6 Physical Interpretation

Low-SFE (Al-rich) alloys favor deformation twinning and high strain hardening, whereas Mn/Pd-rich alloys with higher SFEs deform mainly by dislocation slip—linking atomic-scale energies with macroscopic mechanical response.

### 4.7 Reproducibility and Automation

All simulations were automated using Python scripts for structure generation, job execution, and data extraction, ensuring consistency, scalability, and easy reproducibility.

### 4.8 Overall Outcome

Even though the results were not perfectly accurate, the process was highly educational and enjoyable. I gained confidence in working with atomistic simulations, analyzing energy trends, and understanding the physical meaning of stacking fault energies in alloy systems.

## References


1. M. A. Charpagne, K. V. Vamsi, Y. M. Eggeler, S. P. Murray, C. Frey, S. K. Kolli, T. M. Pollock, "Design of Nickel–Cobalt–Ruthenium multi-principal element alloys," *Acta Materialia*, 194 (2020) 224–235.
2. *ASM Handbook, Volume 3: Alloy Phase Diagrams*, ASM International (1992).
3. J. A. Zimmerman, C. L. Kelchner, P. A. Klein, J. C. Hamilton, S. M. Foiles, "Generalized stacking fault energies for embedded-atom FCC metals," *Modelling and Simulation in Materials Science and Engineering*, 8 (2000) 103–115.
4. *NIST Interatomic Potentials Repository*, Available at: `https://www.ctcms.nist.gov/potentials/`
5. Schopf, N., et al., "EAM Potential for Al–Mn–Pd System (AlMnPd_Schopf_2012.lammps.EAM_CORRECT)," NIST Interatomic Potentials Repository (2012). Available at: `https://www.ctcms.nist.gov/potentials/`